13

Application of Moire Interferometry to Strain Analysis of PCB Deformations at Low Temperatures

Arkady Voloshin

Department of Mechanical Engineering and Mechanics, Lehigh University, Bethlehem, PA 18015, USA

Abstract Microelectronics packaging has been developing rapidly over the past ten years due to the demands for faster, lighter and smaller products. Printed circuit boards (PCBs) provide mechanical support and electrical interconnection for electronic devices. Many types of composite PCBs have been developed to meet various needs. Recent trends in reliability analysis of PCBs have involved developing of the structural integrity models for predicting lifetime under thermal environmental exposure; however the theoretical models need verification by the experiment.

The objective of the current application is the development of an optical system and testing procedure for evaluation of the thermal deformation of PCBs using moire interferometry. Due to the special requirements of the specimen and test condition, the existing technologies and setups were updated and modified. The discussions on optical methods, thermal loading chambers, and image data processing are presented. The proposed technique and specially designed test bench were employed successfully to measure the thermal deformations of PCB in the temperature range of $-40°C$ to $+160°C$. The video-based moiré interferometry was used for generating, capturing and analysis of the fringe patterns. The obtained information yields the needed coefficients of thermal expansion (CTE) for tested printed circuit boards.

13.1. INTRODUCTION

Printed circuit boards (PCBs) consist of one or more layers of metal, bonded onto insulating substrates that are fabricated from the glass-fiber-reinforced thermosetting resin. Thermal stresses in microelectronics interconnections are developed due to mismatch of the coefficient of thermal expansion (CTE) between the package and substrate. Accurate measurements of the PCB thermal deformation will provide actual values for the CTE which is of importance for reliability assessment of the microelectronics assembly.

Number of optical methods such as shadow moiré [1–3], differential interferometry [4], optical profilometry [5], Fizeau interferometry [6], electronic speckle pattern inter-

ferometry [7,8], digital speckle correlation [9,10], and moiré interferometry, described in details by D. Post et al. [11], are available for experimental evaluation of the deformations. Some of these, like shadow moiré, electronic speckle pattern interferometry and digital speckle correlation, do not provide the necessary deformation resolution, while others require specialize equipment and knowledge for use.

Compared with other, the moiré interferometry is an ideal optical technique for high resolution, non-contact and full-field deformation measurements. Some measurements of the CTE by using moire interferometry have been reported [12–14], and the test results were in good agreement with other methods, such as strain gage techniques. These reports were for the temperature range from +20°C to around +110°C only. However, higher temperatures occur in the reflow process and in some application, e.g., under the hood electronic devices. When the PCB substrate material is heated above T_g (glass transition temperature), it behaves as an elastomer. The manufacturers are trying to develop PCBs with high T_g. However, in the meantime, it will be helpful if the test data for the organic substrate can be provided near or above T_g. Low temperature also might be encountered in storage, shipping or operation of the electronics components. Almost all reliability testing standards for microelectronics require the temperature cycling down to −40°C or lower, but few studies appear to have been done at these temperature ranges. A real time low temperature test of PCBs will provide useful information about their behavior. As a composite structure made of organic thermosetting resin, woven fiberglass and copper foil, used as inner-layer, the PCB's dimensional stability is significantly impacted by any temperature change. Initial surface irregularities and deformation, residual stress, free-edge effect and fixture mode of specimen may have a significant influence on the test results. Finally, several technical issues have to be resolved in the practice of specimen grating application, optical interferometry setup, experimental arrangement and data processing.

The present chapter discusses the technical concerns, describes the experimental procedure and presents results for four types of PCBs. The thermoelastic properties (coefficient of thermal expansion) were measured in both the warp and the fill directions. Samples were made of a common, commercially pressed core (2116) woven glass epoxy substrate sandwiched between copper cladding. Obtained results show the viability of methodology presented here for CTE measurements in the wide temperature range. The obtained data can be used in the models for predicting the reliability of the microelectronics packages.

13.2. OPTICAL METHOD AND RECORDING OF FRINGE PATTERNS

One of the most intriguing problems in experimental mechanics is the accurate measurement of relatively small deformations without applying too much change to the specimen's stiffness. This quest brought the development of the so called moire method. The idea is extremely simple: attach a very low stiffness grating to the sample surface and monitor its deformation due to the loads experienced by the sample. The direct monitoring of the grating is called a "grid" method, which has some merits, but suffers from low sensitivity [15]. But even the moire method, that is based on interference of the two gratings: "master" and "specimen," as late as up to 1960's had a limited resolution since the technique was limited to gratings of up to 30–40 lines/mm. Such systems allowed measurement of strains in the several percent range. To overcome this limitation one may pursue either increase in the number of lines per unit length or devise methods that will allow extracting information not only from the full fringe values, but also work with the fractional fringes.

The review of the moire history shows that researches pursued both avenues with significant success. The current systems allow measurement of strains on the order 20 microstrains, i.e., 500-fold improvement in the sensitivity of moire method.

13.2.1. Fractional Fringe Approach

Moiré pattern characterizes the displacement at every point on the specimen surface. By using digital image analysis and fractional fringe analysis techniques [16], the displacement can be computed at every location throughout the moire pattern. This is accomplished by utilizing a basic optical law [17] that relates light intensities in a moiré field to the corresponding displacements as

$$W(x, y) = W_0 + 1/2\pi \cdot f \cdot \arccos[(I(x, y) - I_0)/I_1], \tag{13.1}$$

where W_0 is the displacement at some starting point, f is the frequency of the grating, $I(x, y)$ is the light intensity at the point under consideration, I_1 is the intensity amplitude of the first harmonic term in the optical law, and I_0 is the average background light intensity.

Equation (13.1) utilizes only the first term in the series [17], since here one is dealing with nearly pure sinusoidal light intensity distribution due to the nature of the moiré grating. The values of I_1 and I_0 are determined by the image analyzer for each half fringe separately. Since the digital image analyzer has light intensity resolution of 256 gray levels, one can hope for effective fringe multiplication of 512, however in practice multiplication of 20 are more reliable due to inherent optical and electronic noise [18]. This approach is applicable to any moire pattern and is not dependent on the way the pattern produced. It has to be mentioned that the Equation (13.1) deals only with the fractional part of the fringe value. Its integer part W_i has to be established by either manual or automated fringe counting routine.

$$W_i = \frac{N}{f}, \tag{13.2}$$

where $1/f$ is a pitch, or distance between the grating lines at the master and N is the fringe number.

13.2.2. Grating Frequency Increase

As it is mentioned above, the alternate approach to increase the sensitivity of the moire method is to increase the frequency of the grating. But, here one comes to the problem of the diffraction effects. An effective way to overcome this is to produce a so called “phase grating” that effectively did not absorb light. This became possible due to availability of newly developed techniques used in the microelectronic industry. As result, gratings with frequency of 2240 lines/mm were produced already in 1973 [19]. To apply these gratings to the specimen surface, a replication technique was developed [20] that is used by nearly every practitioner of moire interferometry. Thus, the problem of high-frequency specimen grating was solved. The next challenge was creation of a high-frequency master grating.

13.2.3. Creation of a High-Frequency Master Grating

Moire interferometry allows operation with a very small grating pitch. The interference pattern formed by a pair of collimated coherent light beams, C′ and D′, interacting at angles $+\alpha$ and $-\alpha$, is used as a virtual master grating (Figure 13.1). The frequency of reference grating is

$$f = \frac{2}{\lambda} \sin \alpha, \tag{13.3}$$

where λ is the wavelength of the beam. The initial frequency of the specimen grating, f_s, is chosen to be half of the virtual reference grating f. The sensitivity of the measurements is controlled by f.

The ±45° adjustable mirrors direct portions A′ and B′ of the collimated beam to angle $+\alpha$ and $-\alpha$ in the vertical plane. They form a virtual reference grating with its grating lines perpendicular to the y axis; it interacts with the corresponding specimen grating lines to form the V field. When light from A′ and B′ is blocked, beams from C′ and D′ form the U field (Figure 13.1). The system does not need a polarizing filter, however, a larger collimated input beam (> ∅ 100 mm) is required. The wavelength of the light 0.6328 μm and $\alpha = 49.4°$ results in $f = 2400$ line/mm. Thus, each fringe represents an in-plane displacement of $1/f = 416$ nm in this study.

When moire is used for deformation studies, the location of the zero-order fringe is arbitrary since any rigid-body translations are not importance for strain analysis. What is important is relative displacement and not the absolute value. Several rules have to be observed when assigning the values to visible moire fringes. Adjacent fringes differ by one fringe order, either up or down. However, in the areas of local maxima or minima the adjacent full fringes may be assigned the same order since the local extremum maybe located in between the full fringe values. Fringes of unequal orders can not intersect.

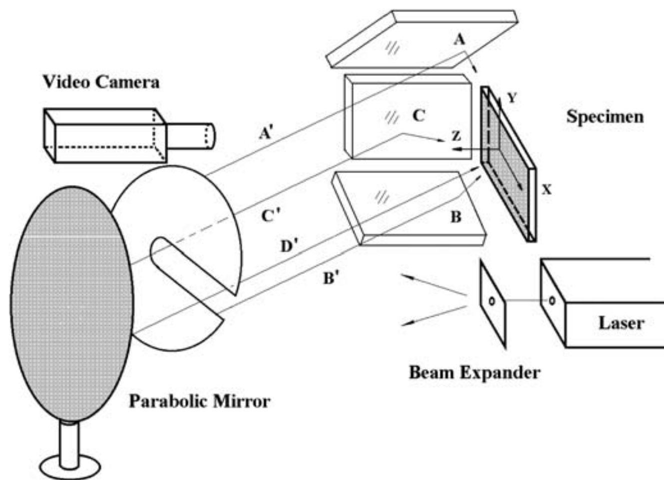

FIGURE 13.1. Four beam moiré interferometry.

Since we are looking for deformations, it is obvious that only derivatives of the displacements are of interest.

$$\varepsilon_x = \frac{\partial W_x}{\partial x} \quad \text{and} \quad \varepsilon_y = \frac{\partial W_y}{\partial y}. \tag{13.4}$$

In order to get the correct strain value sign, it is important to establish the direction of the positive strain gradient. After selecting the coordinate system, one has to assign fringe values in such a way that the derivative of the fringe number along the positive x or y direction will result in correct sign for the strain.

In cases where the sign of the gradient is not known a priori it may be established by an simple experiment. Apply the small displacement to the specimen while observing the fringe pattern. If the displacement is in the positive x direction, the fringe orders will all increase, i.e., fringes will move in the direction of the lower fringe value. For a negative fringe gradient, fringes will move in the same direction as displacement applied to the specimen.

13.2.4. Combination of the High Grating Frequency and Fractional Fringe Approach

The above combination allows significant increase in the deformation measurement sensitivity. The developed hardware-software combination resulted in a systems capable resolve displacement as low as 20 nm. This wining combination becomes a standard way to study the deformations in the systems that could never be approached even 20 years ago. The contemporary systems consist of the environmental chamber with the sample, mirror holders and camera stage. These elements were attached to a solid base plate, which makes the optical assembly stable and robust. The developed system produces exceptionally stable fringes under thermal and mechanical loading. SONY® XC-75 CCD video camera was used to capture the real time fringe patterns. An analog video output signal was saved on the video tape, later converted into an 8-bit digital signal and stored in a PC in the form of a 640 × 480 pixels picture for further processing. The linear scale for all measurements was in the range of 0.010 to 0.024 mm/pixel.

13.3. DATA PROCESSING

The moiré patterns were recorded during thermal loading and processed off-line. These patterns had sufficient number of fringes in order to use a simple fringe counting; there was no need to utilize any of the techniques for fractional fringe analysis [21]. The data processing was performed by a routine written in MATLAB®. Each moiré image was scanned along several selected sections; number of full fringes was automatically detected, multiplied by the pitch (416 nm) to represent the displacement along the scan line. The straight line was fitted to the obtained displacement; its slope represented the average strain along this section.

13.4. TEST BOARDS AND SPECIMEN GRATING

Etched or unetched copper (CU) panels and adhesive prepregs (type 2116) were laminated, pressed and cured to produce a rigid PCB board of the desired configuration. Four

types of PCB configurations were prepared for this study. The samples of the PCBs for testing were cut to the size of 34 × 28 mm. The warp and fill directions are corresponding to the x and y axes as shown in Figures 13.2–13.4. Each board contained various number of prepreg and CU layers as described below.

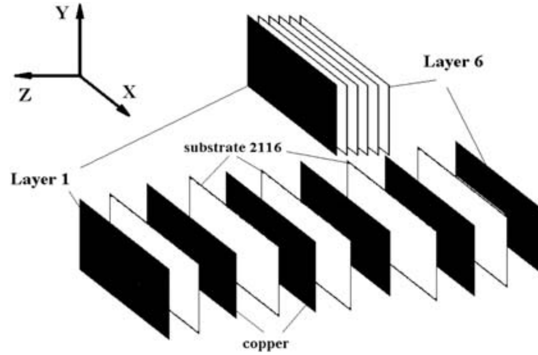

FIGURE 13.2. Configuration of board B.

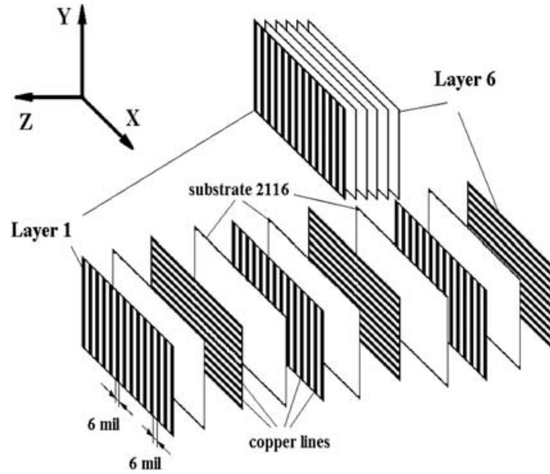

FIGURE 13.3. Configuration of board C.

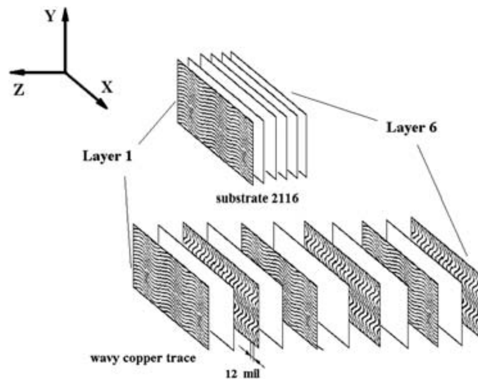

FIGURE 13.4. Configuration of board D.

Board A: 5 layers of the prepreg 2116, the final thickness was 1.14 mm;
Board B: 6 full CU layers and 5 layers of the prepreg 2116, final thickness was 1.36 mm;
Board C: 6 layers of straight copper traces (152.4 μm line width, and 152.4 μm space between lines and 5 layers of the prepreg 2116, adjacent copper layers have traces in alternating directions), final thickness was 1.25 mm;
Board D: 5 layers of the prepreg 2116 with wavy copper traces (152.4 μm line width, and 152.4 μm space between lines, adjacent copper layers have traces in alternating direction, the amplitude and wavelength of the waviness was 0.305 mm and 2.5 mm). Its final thickness was 1.25 mm.

The configurations of the last three types of test boards are shown in Figures 13.2–13.4.

A 1200 line/mm crossed-line grating was first replicated onto an 87 × 75 × 5.7 mm glass plate, which was coated with a reflective aluminum film by evaporation using Denton® DV-502A system. This grating was replicated on the specimen surface at room temperature. The specimen was then placed inside the environmental chamber. Three K type thermocouple probes were attached to the specimen to monitor its temperature during the test. The differences between the thermocouples were under 0.8°C.

13.5. ELEVATED TEMPERATURE TEST

The heat source was a resistance heater attached to the heat sink built into the chamber. Typical temperature profile is shown in the Figure 13.5 (the heat loading rate was about 2.9° C/min).

The mirrors were adjusted to provide a null field. However it is nearly impossible to get a true null field, this is especially complicated task for the four beam moiré interferometry. Thus, the initial moiré patterns were recorded and used later as a basis for analysis. The optical data was continuously recorded by a VCR during test. After the end of data acquisition, number of frames representing PCB thermal deformation at selected temperatures was selected; moiré fringe patterns were digitized by a frame grabber (MATROX Meteor II) and stored for data processing. Each frame was later scanned along vertical and horizontal sections to extract the pertinent displacement data for each increment of temperature.

If the specimen would have a uniform CTE and would be subjected to a homogeneous temperature field, the moiré fringe field would appear as uniformly spaced, parallel, straight

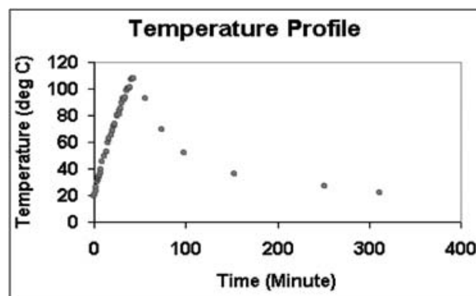

FIGURE 13.5. Typical heat loading history.

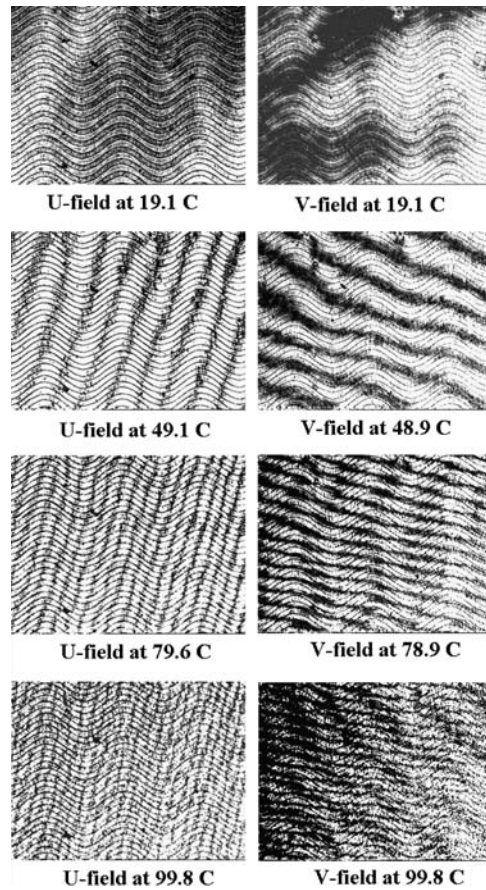

FIGURE 13.6. Temperature dependent moiré fringe patterns for board D.

lines—vertical lines for the horizontal or U-displacement field and horizontal lines for the vertical or V-displacement field. However, the null field and surface irregularity of PCB made the fringe patterns somewhat tilted.

Typical U and V-field fringe patterns for the board D are shown in Figure 13.6 for a range of temperatures. The scan lines used for analysis of the moiré fringe patterns are shown in Figure 13.7.

Scan lengths for U-field and V-field were 6.78 and 4.67 mm, respectively. Light intensity along the scan lines was acquired by a MATLAB routine and position of the full fringes were detected automatically. They were numbered consequently since the deformation was either uniform extension (heating) or uniform compression (cooling). The average temperature induced strain was obtained from a numerical derivative of the measured displacement vs. position. This process was repeated at about 10–15 different temperatures. The obtained data—measured average strain as a function of temperature—is shown in Figure 13.8 for each type of the measured boards. Slope of the data curve provides values for the apparent coefficients of thermal expansion in x and y directions. The first order curve was fitted to the data; the equation can be seen in each of the plots (Figure 13.8). The coefficient in front of "x" represents the slope of the line, i.e., the measured coefficient of thermal extension for the given test.

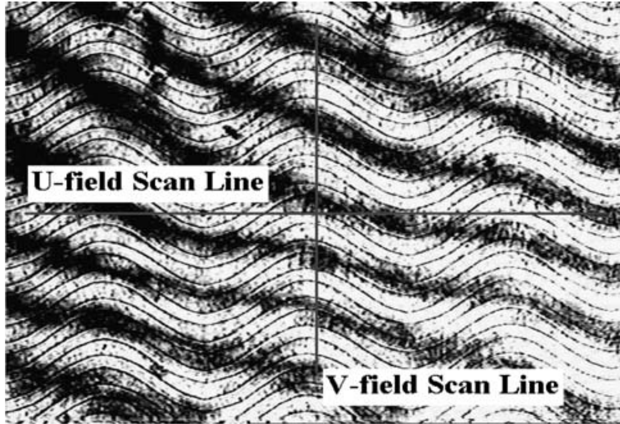

FIGURE 13.7. Scan lines location.

Thermal Expansion along X Axis (Board A)
y = 1.643E-05x - 2.069E-04
Average Strain: 0, 0.0002, 0.0004, 0.0006, 0.0008, 0.001, 0.0012, 0.0014, 0.0016
Temperature (C): 0, 20, 40, 60, 80, 100, 120

Thermal Expansion along Y Axis (Board A)
y = 1.558E-05x - 2.077E-04
Average Strain: 0, 0.0002, 0.0004, 0.0006, 0.0008, 0.001
Temperature (C): 0, 10, 20, 30, 40, 50, 60, 70, 80

Thermal Expansion along X Axis (Board B)
y = 1.730E-05x - 2.330E-04
Average Strain: 0, 0.0005, 0.001, 0.0015, 0.002, 0.0025, 0.003, 0.0035
Temperature (C): 0, 50, 100, 150, 200, 250

Thermal Deformation along X Axis (Board B, Cooling)
y = 1.722E-05x - 2.045E-04
Average Strain: 0, 0.0005, 0.001, 0.0015, 0.002, 0.0025, 0.003, 0.0035
Temperature (C): 250, 200, 150, 100, 50, 0

Thermal Expansion along X Axis (Board C)
y = 1.645E-05x - 2.775E-04
Average Strain: 0, 0.0002, 0.0004, 0.0006, 0.0008, 0.001, 0.0012
Temperature (C): 0, 10, 20, 30, 40, 50, 60, 70, 80, 90

Thermal Expansion along Y Axis (Board C)
y = 1.716E-05x - 2.815E-04
Average Strain: 0, 0.0004, 0.0008, 0.0012, 0.0016, 0.002
Temperature (C): 0, 20, 40, 60, 80, 100, 120

FIGURE 13.8. Temperature dependent strain.

TABLE 13.1.
Test results.

Test board		CTE (ppm/°C)	
		Warp direction	Fill direction
A	2116	17.2 ± 0.3	16.8 ± 0.3
B	2116 with full Cu	18.2 ± 0.4	18.0 ± 0.3
C	2116 with straight Cu traces	18.5 ± 0.3	18.4 ± 0.4
D	2116 with wavy Cu traces	17.6 ± 0.4	16.9 ± 0.4

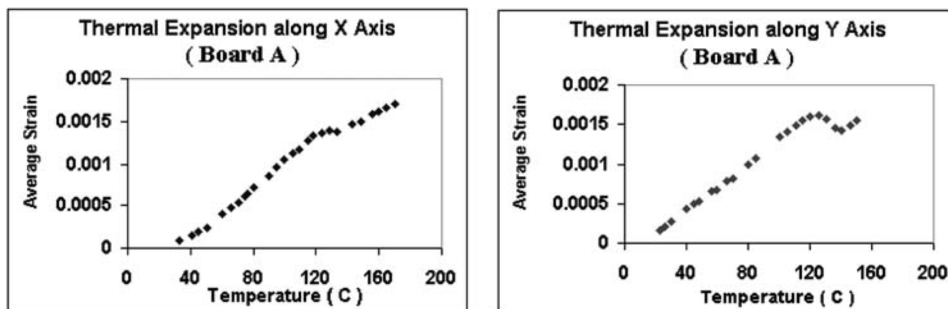

FIGURE 13.9. Test board A (25–160°C).

The presented data demonstrates that the thermal expansion of PCB boards is basically linear from the room temperature to +110°C. The data was recorded both during the heating up (+20 to +110°C) and cooling down (+110 to +20°C) of the board. The obtained results did not differ significantly, as may be seen from the data for "board B" (Figure 13.8). The CTEs were not significantly different in the wrap and fill directions, as may be seen in the Table 13.1.

The data presented in Table 13.1 was acquired for the temperature range of room to +1100°C. This range is still below the glass transition temperature, T_g. Above +1100°C the *in-situ* fringe patterns became not very clear, mainly due to moisture accumulation on the glass window of the environmental chamber.

To study the board behavior at higher temperatures, a single window glass was replaced by a double layer glass window. This modification allowed increasing the temperature in the chamber up of +160°C; at higher temperatures the specimen grating became damaged. The test results for the board A are presented in Figure 13.9. It is obvious that the glass transition temperature for this specimen is in the range of +120°C to +130°C. The CTE in the X and Y directions usually decreases above the T_g, as it is seen in Figure 13.9, mainly due to the resin modulus decrease. The effect of the fiber reinforcement becomes stronger since its modulus is relatively unaffected by the higher temperature.

13.6. LOW TEMPERATURE TEST

The sample preparation for low temperature test was done in the same manner as for the elevated temperature test. The specimen grating was replicated at the room temperature and the sample was placed in the environmental chamber. It was built to provide a range

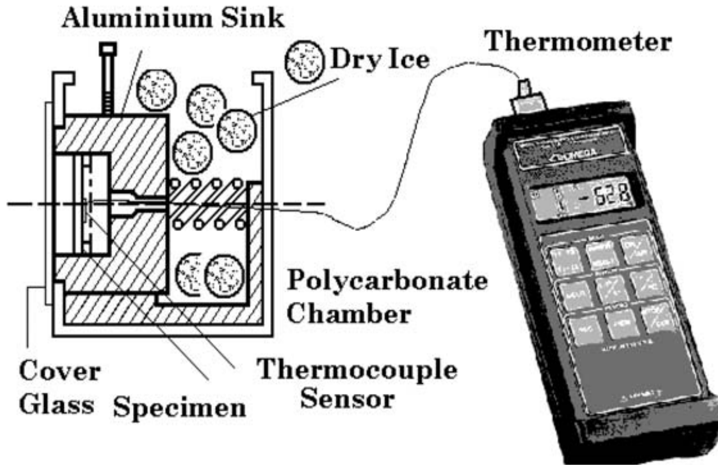

FIGURE 13.10. Cooling chamber.

of temperatures from the room to −40°C. Several cooling methods were evaluated for the applicability and convenience.

The liquid nitrogen (−196°C) can provide fast and efficient cooling loading, but boiling will result in the chamber tremble, which may be detrimental for the optical testing. Thermoelectric coolers (TECs) are solid state heat pumps that utilize the Peltier effect. However, high performance of these coolers can not be achieved without developing and building a custom TEC setup.

Dry ice, frozen carbon dioxide (CO_2), also can be used for cooling since its temperature is −78.5°C. Cooling by dry ice is safe, environmentally clean and easy to control. A specially designed chamber (Figure 13.10) capable of holding up to one kilogram of dry ice was built. This quantity was sufficient to cool the chamber and the sample to the needed temperature of −40°C.

The heat sink was made of aluminum. Kodak projector slide cover glass (102 × 83 × 1.2 mm) was used to build a four layer glass window. Multi-layer glass window was needed for two reasons: to prevent the fogging and to reduce the heat loss. The mist on the outside glass layer was wiped out by the Varitemp® heat gun.

Dry ice was placed into the chamber and the optical setup was adjusted to get the parallel null field fringe pattern. The data recording was initiated. It went from the room temperature to −40°C, the cooling phase took about 30–40 minutes (Figure 13.11, Mode I); the data recording continued until the sample reached the room temperature again (Mode II). During thermal loading process the temperature gradient was between 2°C/min to less than 0.2°C/min.

Fringe patterns and corresponding temperatures were recorded and processed offline. The typical moiré patterns and the temperature dependent average strain for the Mode I are shown for all four boards (Figures 13.12–13.15).

The CTEs of all boards were basically constant, with values of 16–18 ppm/°C in the range of −40°C to +20°C. The results were in agreement with those recorded in the temperature range of +20°C to +110°C.

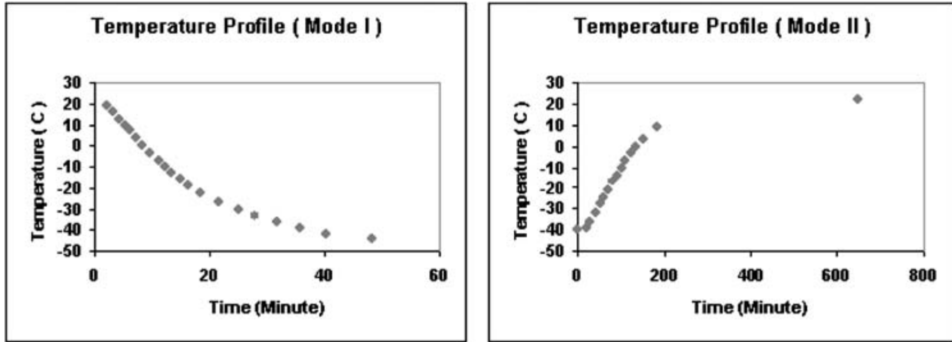

FIGURE 13.11. Two modes of cooling.

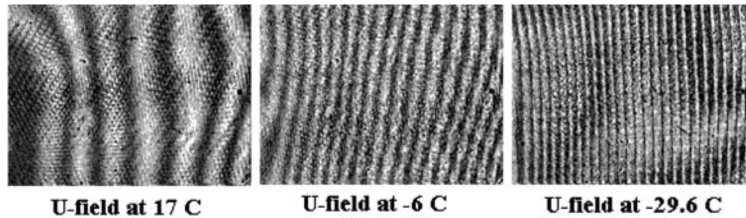

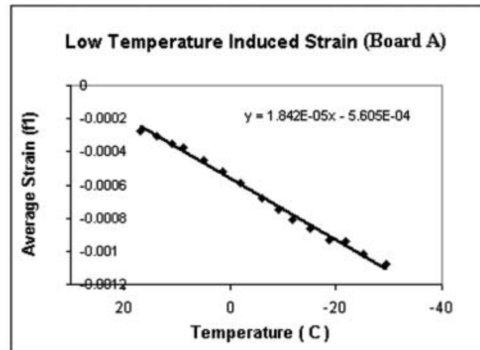

FIGURE 13.12. Cooling test result of board A.

13.7. CONCLUSIONS

Despite the wide proliferation of the finite element and other procedures capable to model the thermal behavior of the complex printed circuit boards, still here is a need to measure the deformations experienced by the PCB under various thermal loadings. To fully understand the nature of these deformations full-field methods are necessary. One of the most successful candidates for this task became the moire interferometry method for real-time deformation measurements. This method provide high special resolution, the displacement on the order of 20 nm are measured along the scan lines up to 10 mm long. It is applicable to study in-plane and out-of plane deformations. The main restriction is that the starting surface has to be reasonable flat, how flat depends on the required resolution.

A robust scheme of moiré interferometry for real-time observation of thermal deformations was described here. The scheme was implemented with both high and low tem-

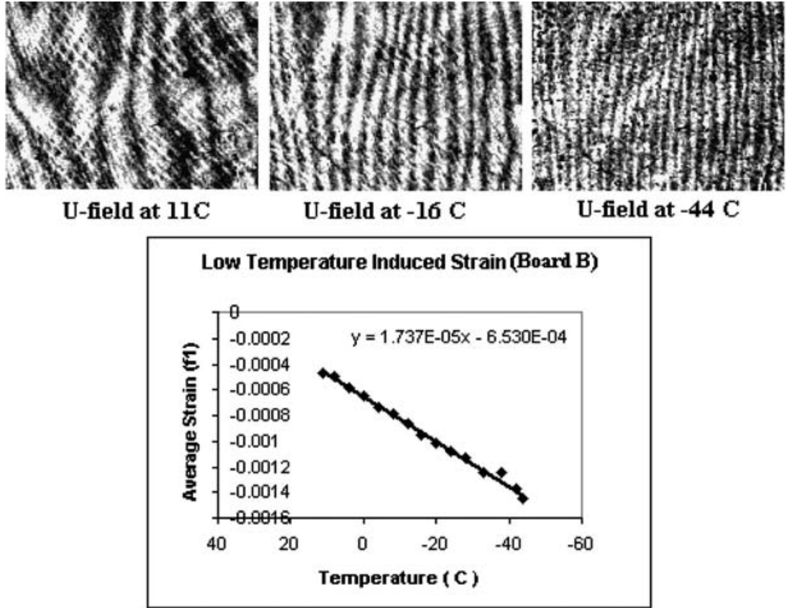

FIGURE 13.13. Cooling test result of board B.

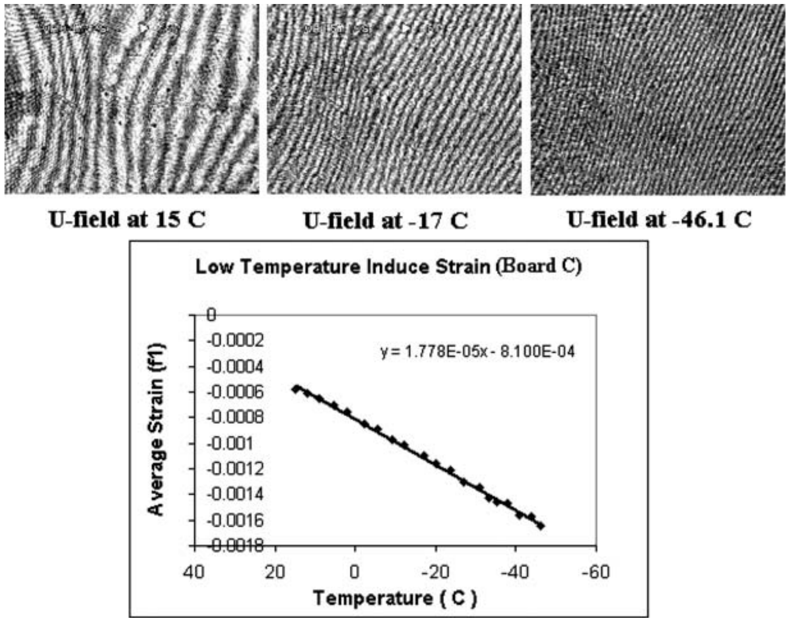

FIGURE 13.14. Cooling test result of board C.

perature environmental chambers that produce temperature profiles needed for the thermal testing. The in-plane deformations of the four types of PCBs were measured in the −40 to +160°C range. The test results show that the CTE of all boards are basically con-

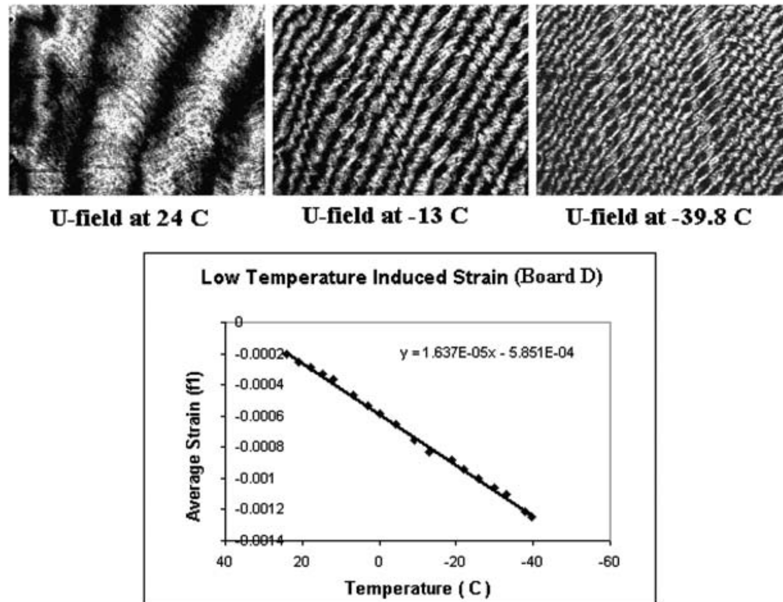

FIGURE 13.15. Cooling test result of board D.

stant from −40°C to T_g, with values of 16–18 ppm/°C. It is the first work describing the *in-situ* measurements of the PCBs coefficient of thermal expansion in the low temperature range (−40°C).

The system described here was successful for the thermal-mechanical behavior measurement of PCB specimens in the wide temperature range. The obtained data may be used for verification of the numerical procedures used for prediction of the CTE for the complicated PCBs arrangements. They also may be useful for prediction of the PCB lifetime under various thermal environments.

The main drawback of this technique is that there are no commercially available systems that allow a user to place a sample, push a button and get the results. Significant preparation is required to get the moire patterns and not less effort is needed for proper interpretation of the recorded images. But, these difficulties are justified by the wealth of full-field data obtained from the real samples under real thermal loads.

ACKNOWLEDGMENT

This research was supported by the Pennsylvania Department of Community and Economic Development for the program "Miniaturized Electronics" (Contract No. 20-906-0015) which was administered through an Alliance of Visteon Systems, LLC, Lehigh and Penn State Universities. Special thanks go to Dr. Terence Clark and Larry Schmidt at Visteon for fruitful discussions, as well as to Dr. Terence Clark for program coordination.

REFERENCES

1. Y. Wang and P. Hassell, Measurement of thermally induced warpage of BGA packages/substrates using phase-stepping shadow moiré, Proc. of the 1st Electronic Technology Conference, 1997, pp. 283–289.
2. K. Verma, D. Columbus, B. Han, and B. Chandran, Real-time warpage measurement of electronic components with variable sensitivity, 1998 Electronic Components and Technology Conference, 1998, pp. 975–980.
3. P.B. Hassell, Advanced warpage characterization: location and type of displacement can be equally as important as magnitude, Proc. of Pan Pacific Microelectronics Symposium Conference, Feb. 2001.
4. S. Dilhaire, T. Phan, E. Schaub, and W. Claeys, High sensitivity and high resolution differential interferometer: micrometric polariscope for thermomechanical studies in microelectronics, Microelectronics Reliability, 37(10/11), pp. 1587–1590 (1997).
5. C.W. Tsai, C.H. Lee, and J. Wang, Deconvolution of local surface response from topography in nanometer profilometry with a dual-scan method, Optics Letters, 24(23), pp. 1732–1734 (1999).
6. K. Verma, D. Columbus, and B. Han, Development of real time/variable sensitivity warpage measurement technique and its application to plastic ball grid array package, IEEE Transactions on Electronics Packaging Manufacturing, 22(1), pp. 63–70 (1999).
7. T. Ahrens and M. Krumm, Deformation measurement at components, printed wiring boards and microelectronic assemblies to ensure the reliability of a system, Proceedings of EUPaC'96, 2nd European Conference on Electronic Packaging Technology, 1996, pp. 108–112.
8. K.-S. Kim, J.-H. Kim, J.-K. Lee, and S.-S. Jarng, Measurement of thermal expansion coefficients by electronic speckle pattern interferometry at high temperature, Journal of Materials Science Letters, 16(21), pp. 1753–1756 (1997).
9. Y.C. Chan and F. Yeung, Nondestructive detection of defects in miniaturized multilayer ceramic capacitors using digital speckle correlation techniques, IEEE Transactions on Components, Packaging, and Manufacturing, Part A, 18(3), pp. 677–684 (1995).
10. H. Lu, C. Yeh, and K. Wyatt, Experimental evaluation of solder joint thermal strain in a CSP using digital speckle correlation, 1998 InterSociety Conference on Thermal Phenomena, 1998, pp. 241–245.
11. D. Post, B. Han, and P. Ifju, High Sensitivity Moire, Spring-Verlag, New York, 1994.
12. T. Ratanawilai, B. Hunter, G. Subbarayan, and D. Rose, A comparison between moire interferometry and strain gages for effective CTE measurement in electronic packages, 2000 InterSociety Conference on Thermal Phenomena, 2000, pp. 246–252.
13. A.F. Bastawros and A.S. Voloshin, Transient thermal strain measurements in electronic packages, IEEE Transactions on Components, Hybrids and Manufacturing Technology, 13(4), pp. 961–966 (1990).
14. B. Han, Z. Wu, and S. Cho, Measurement of thermal expansion coefficient of flexible substrate by moire interferometry, Experimental Techniques, 25(3), pp. 22–25 (2001).
15. A.J. Durelli and W.F. Riley, Development in the grid method of experimental stress analysis, Proc. SESA, XIV(2), pp. 91–100 (1957).
16. A.S. Voloshin, C.P. Burger, R.E. Rowland, and T.S. Richard, Fractional moire strain analysis using digital imaging technique, Experimental Mechanics, 26, pp. 254–258 (1986).
17. C.A. Sciammarella, Basic optical law in the interpretation of moire pattern applied to the analysis of strain—Part I, Experimental Mechanics, 5, pp. 154–160 (1965).
18. A.F. Bastawros and A.S. Voloshin, Thermal strain measurements in electronic packages through fractional moiré interferometry, Journal of Electronic Packaging, 112, pp. 303–308 (1990).
19. K. Kato, F. Yamato, T. Murota, and T. Jimma, Improvement on method of measuring strain using interference fringes of diffracted beams at gratings on specimens, Bull. JSME, 16(100), pp. 1513–1523 (1973).
20. D. Post and W.A. Baracat, High sensitivity moire interferometry—a simplified approach, Experimental Mechanics, 21(3), pp. 100–104 (1981).
21. A.S. Voloshin, P.H. Tsao, and R.A. Pearson, In situ evaluation of residual stresses in an organic die-attach adhesive, Journal of Electronic Packaging, 120(3), pp. 314–318 (1998).